

Self-Organized Criticality in Solar and Stellar Flares: Are Extreme Events Scale-Free ?

Markus J. Aschwanden¹

¹) *Lockheed Martin, Solar and Astrophysics Laboratory, Org. A021S, Bldg. 252, 3251 Hanover St., Palo Alto, CA 94304, USA; e-mail: aschwanden@lmsal.com*

ABSTRACT

We search for outliers in extreme events of statistical size distributions of astrophysical data sets, motivated by the *Dragon-King hypothesis* of Sornette (2009), which suggests that the most extreme events in a statistical distribution may belong to a different population, and thus may be generated by a different physical mechanism, in contrast to the strict power law behavior of *self-organized criticality (SOC)* models. Identifying such disparate outliers is important for space weather predictions. Possible physical mechanisms to produce such outliers could be generated by sympathetic flaring. However, we find that Dragon-King events are not common in solar and stellar flares, identified in 4 out of 25 solar and stellar flare data sets only. Consequently, small, large, and extreme flares are essentially scale-free and can be modeled with a single physical mechanism. In very large data sets ($N \gtrsim 10^4$) we find significant deviations from ideal power laws in almost all data sets. Nevertheless, the fitted power law slopes constrain physical scaling laws in terms of flare areas and volumes, which have the highest nonlinearity in their scaling laws.

Subject headings: Sun: corona — Sun: flares — Sun: X-rays, gamma rays — stars: flare — methods: statistical

1. INTRODUCTION

The largest natural catastrophes that can happen are obviously of highest interest, because they cause the largest threats and damages, such as the biggest earth quakes, land slides, wild fires, volcanic eruptions, terrorist attacks, stock market crashes, solar flares, coronal mass ejections, or magnetospheric storms (see reviews and textbooks by Bak 1996; Jensen 1998; Charbonneau et al. 2001; Hergarten 2002; Sornette 2004; Aschwanden 2011, 2013; Aschwanden et al. 2016; Pruessner 2012; Watkins et al. 2016; Sharma et al. 2016). The ubiquitous power law-like size distributions that are universally found in the statistics of event sizes have been attributed to nonlinear scale-free processes. The observed size distributions can generally be subdivided into three regimes: (i) a range of incomplete sampling below the inertial range, (ii) an inertial range over which the power law function holds, and (iii) a cutoff above the inertial range that approaches effects of the finite system size. The three regimes can be associated with (i) small events, (ii) large events, and (iii) extreme events. Generally, it is tacitly assumed that small, large, and extreme events belong to the same population, the same category of events, and be driven by the same physical event generation mechanism (for a given phenomenon). However, it has recently been suggested that the most extreme events do not develop similarly to the other events, at least for the case of stock market crashes, which are predictable to some extent based on their precursor behavior, a phenomenon that has been dubbed the “*Dragon-King hypothesis*” (Sornette 2009; Sornette and Ouillon 2012). This hypothesis suggests that extreme events may

result from amplification and synchronization processes, and that the “*Big events*” do have characteristic fingerprints enabling their forecasting and prediction. Another application of this hypothesis is the sub-critical failure of materials under load, where a long phase of damage accumulation characterized by power law distributed microfracture events finally give way to catastrophic breakdown (Baro et al. 2013). A third application are magnetospheric storms, where a growing recognition emerges that long-range correlations are an essential feature of systems that exhibit extreme events (Sharma 2017). In this study we investigate the question whether extreme events of solar and stellar flares are consistent with a power law distribution as an extension of a scale-free inertial range, or if they show significant deviations from ideal power laws.

2. DATA ANALYSIS AND RESULTS

2.1. Definition of Power Law Distributions

An ideal power law distribution that represents a *differential occurrence frequency distribution*, also simply called a *size distribution* $N(x)$ of events, as a function of some size parameter x , can be described by four parameters $(x_1, x_2, n_0, \alpha_x)$,

$$N(x)dx = n_0 x^{-\alpha_x} dx, \quad x_1 \leq x \leq x_2, \quad (1)$$

where x_1 and x_2 are the lower and upper bounds of the power law inertial range, α_x is the power law slope, and n_0 is the normalization constant,

$$n_0 = n_{ev}(1 - \alpha_x) [(x_2)^{1-\alpha_x} - (x_1)^{1-\alpha_x}]^{-1}. \quad (2)$$

with n_{ev} being the total number of events contained in the inertial range $[x_1 \leq x \leq x_2]$.

The ideal power law function (Eq. 1) can be generalized with an additional “shift” parameter x_0 (with respect to x), also called *Lomax distribution* (Lomax 1954), *Generalized Pareto distribution* (Hosking and Wallis 1987), or *Thresholded power law size distribution* (Aschwanden 2015),

$$N(x)dx = n_0 (x_0 + x)^{-\alpha_x} dx, \quad (3)$$

with the normalization constant n_0 for the range $x_1 \leq x \leq x_2$,

$$n_0 = n_{ev}(1 - \alpha_x) [(x_2 + x_0)^{1-\alpha_x} - (x_1 + x_0)^{1-\alpha_x}]^{-1}. \quad (4)$$

This additional parameter x_0 accomodates three different features: truncation effects due to incomplete sampling of events below some threshold (if $x_0 > 0$), incomplete sampling due to instrumental sensitivity limits (if $x_0 > 0$), or subtraction of event-unrelated background (if $x_0 < 0$), as it is common in astrophysical data sets.

While Eqs. (1) and (3) represent *differential size distributions* $N_{diff}(x)$, it is statistically more advantageous to employ *cumulative size distributions* $N_{cum}(x)$, especially for small data sets and near the upper cutoff, where we deal with a small number of events per bin. We will use cumulative size distributions that include all events accumulated above some size x , such as for the *ideal power law function*,

$$N_{cum}(x)dx = \int_x^{x_2} n_0 x^{-\alpha_x} dx = 1 + (n_{ev} - 1) \left(\frac{x_2^{1-\alpha_x} - x^{1-\alpha_x}}{x_2^{1-\alpha_x} - x_1^{1-\alpha_x}} \right). \quad (5)$$

or for the *thresholded power law size distribution*,

$$N_{cum}(> x) = \int_x^{x_2} n_0(x + x_0)^{-\alpha_x} dx = 1 + (n_{ev} - 1) \left(\frac{(x_2 + x_0)^{1-\alpha_x} - (x + x_0)^{1-\alpha_x}}{(x_2 + x_0)^{1-\alpha_x} - (x_1 + x_0)^{1-\alpha_x}} \right) . \quad (6)$$

We show an example of a size distribution that contains the counts of events per bin $n_{cts}(x)$ in Fig. (1a), the corresponding differential size distribution $N_{diff}(x) = n_{cts}(x)/\Delta x$ in Fig. (1b), and the corresponding cumulative size distribution $N_{cum}(> x)$ in Fig. (1c). The event count histogram (Fig. 1a) displays the inertial range (x_0, x_2) , the minimum (x_1) , and maximum value (x_2) of the size parameter x , with a peak in the event count histogram at x_0 (Fig. 1a), which provides a suitable threshold definition, because incomplete sampling of small values $x < x_0$ is manifested by the drop of detected events on the left side of the peak x_0 . This definition of a threshold x_0 has been proven to be very useful for characterizing data sets with incomplete or sensitivity-limited sampling (Aschwanden 2015). This provides also a definition for the inertial range (x_0, x_2) , which we will quantify by the number of decades as a logarithmic ratio, i.e., $\log(x_2/x_0)$.

An equivalent method to the cumulative size distribution is the *rank-order plot*. If the statistical sample is rather small, in the sense that no reasonable binning of a histogram can be done, either because we do not have multiple events per bin or because the number of bins is too small to represent a distribution function, we can create a rank-order plot. A rank-order plot is essentially an optimum adjustment to small statistics, by associating a single bin to every event. From an event list of a parameter $x_i, i = 1, \dots, n_x$, which is generally not sorted, we have first to generate a rank-ordered list by ordering the events according to increasing size,

$$x_1 \leq x_2 \leq \dots \leq x_j \leq \dots \leq x_n , \quad j = 1, \dots, n . \quad (7)$$

The bins are generally not equidistant, neither on a linear nor logarithmic scale, defined by the difference between subsequent values of the ordered x_j ,

$$\Delta x_j^{bin} = x_{j+1}^{bin} - x_j^{bin} . \quad (8)$$

In a rank-ordered sequence of n_x events, the probability for the largest value is $1/n_x$, for events that are larger than the second-largest event it is $2/n_x$, and so forth, while events larger than the smallest event occur in this event list with a probability of unity. Thus, the cumulative frequency distribution is simply the reversed rank order,

$$N_{cum}(> x_j) = (n_x + 1 - j) , \quad j = 1, \dots, n_x , \quad (9)$$

and the distribution varies from $N_{cum}(> x_1) = n_x$ for $j = 1$ to $N_{cum}(> x_n) = 1$ for $j = n_x$. We can plot a cumulative frequency distribution with $N_{cum}(> x_j)$ on the y-axis versus the size x_j on the x-axis. The distribution is normalized to the number of events n_x ,

$$\int_{x_1}^{x_n} N(x) dx = N_{cum}(> x_1) = n_x . \quad (10)$$

We overlay rank-order plots in each of the cumulative size distributions in Figs. 1-6 (shown with black diamond symbols), for the $n_{ee} = 10$ most extreme events in every size distribution. If there is a “*Dragon-King*” event, it should manifest itself by a significant offset from the best-fit cumulative size distribution at the upper end in the zone of most extreme events near $x \lesssim x_2$, say by a factor of two at least. The example shown in Fig. 1 exhibits a ratio of $q_{ee} = 1.03$ for the most extreme event, which is a very small offset from the best-fit cumulative size distribution that does not manifest a *Dragon-King* event.

2.2. Least-Square Fits of Size Distributions

In order to test the consistency of the size distribution of extreme events with the size distribution of all events we perform least-square fits of the cumulative size distributions, such as shown in Fig. 1c: the cumulative distribution of an observed parameter x is shown in form of a black histogram with error bars $N_{cum}(> x)$, while the best-fit cumulative size distribution is shown with a red curve (fitted over the range (x_0, x_2) above the threshold), and the extrapolated range below the threshold x_0 is shown with a dashed red curve. We see in Fig. (1c) that the reduced chi-square value is $\chi_{all} = 1.46$ for all events, while the chi-square value is $\chi_{ee} = 0.56$ in the range that contains the $n_{ee} = 10$ most extreme events, and thus is self-consistent between the two ranges, so that we can conclude that the extreme events do not show any significant deviation ($\chi \gtrsim 2$) from the overall (best-fit) thresholded power law distribution in this particular data set.

We estimate the goodness-of-fit from the uncertainties $\sigma_{cum}(x_i)$ of the values $N_i, i = 1, \dots, n_x$ in the fitted size distribution with the standard reduced χ^2 -criterion,

$$\chi_{cum} = \sqrt{\frac{1}{(n_x - n_{par})} \sum_{i=1}^{n_x} \frac{[N_{cum,fit}(x_i) - N_{cum,obs}(x_i)]^2}{\sigma_{cum,i}^2}}, \quad (11)$$

where n_x is the number of bins, $n_{par} = 2$ is the number of free parameters (n_0, a) of the fitted size distribution, $N_{cum,obs}(> x_i)$ is the observed cumulative number of events in each bin, $N_{cum,fit}(> x_i)$ is the fitted cumulative number of events in each bin, and $\sigma_{cum}(x_i)$ is the estimated uncertainty of the cumulative number of events,

$$\sigma_{cum,i} = \sqrt{N_{cum}(x_i) - N_{cum}(x_{i+1})}. \quad (12)$$

This definition is slightly different from the estimate in the previous study (Aschwanden 2015), i.e., $\sigma_{cum,i} = \sqrt{N_{cum,i}}$, which represents a lower limit on the uncertainty only, since the counts of events in each bin are not independent of each other in a cumulative distribution function. Our new approach takes only independent events into account for the estimation of the uncertainty, which in a cumulative distribution is the increment $[N_{cum}(> x_i) - N_{cum}(> x_{i+1})]$, while the remainder of the counts in the bins $N_{cum}(> x_{i+1}), \dots, N_{cum}(> x_{n_x})$ do not vary in the cumulative fit of bin $N_{cum}(> x_i)$, and therefore do not contribute to the uncertainty $\sigma(x_i)$.

Besides the fits of the cumulative size distributions (Fig. 1c), we perform also fits to the differential size distributions for consistency tests (Fig. 1b). Since the differential size distribution is quantified in terms of counts per bin width, $N_{diff}(x) = n_{cts}(x)/\Delta x$, the corresponding χ^2 -criterion is,

$$\chi_{diff} = \sqrt{\frac{1}{(n_x - n_{par})} \sum_{i=1}^{n_x} \frac{[N_{fit,diff}(x_i) - N_{sim,diff}(x_i)]^2}{\sigma_{diff,i}^2}}, \quad (13)$$

and the uncertainty $\sigma_{diff,i}$ in terms of Poisson statistics is,

$$\sigma_{diff,i} = \sqrt{n_{cts}(x_i)/\Delta x_i} = \sqrt{N_{diff}(x_i)\Delta x_i}/\Delta x_i. \quad (14)$$

An example of such a fit is shown in Fig. 1b. Note that the size distribution of the differential size distribution shows a straight power law function even in the range of extreme events, while the cumulative size distribution shows an exponential-like drop-off towards the zero value at x_2 , as a consequence of the integral function defined in Eq. (6). We can compare now the results of the two power law fits and find a power law slope

of $\alpha_{diff,all} = 1.75 \pm 0.02$ for the differential size distribution (Fig. 1b), while the power law slope is $\alpha_{cum,all} = 1.73 \pm 0.02$ for the cumulative size distribution (Fig. 1c). Now, if we inspect the χ^2 -values in the range of the ten most extreme events, we find $\chi_{cum,all} = 1.46$ for all events (above the threshold x_0), and a value of $\chi_{cum,ee} = 0.56$ for the 10 most extreme events (Fig. 1c). Therefore, not only the two methods of differential and cumulative distributions are self-consistent, but the two different ranges (of small-to-large and extreme events) lead to a self-consistent size distribution function also, so that we can conclude that extreme events belong to the same population as all other events, and that no significant deviation from the thresholded power law distribution function is found for this data set, which was obtained from hard X-ray peak photon count rates in solar flares, using the *Hard X-ray Burst Spectrometer (HXRBS)* onboard the *Solar Maximum Mission (SMM)*. The first size distributions of these solar flare data were published in Dennis (1985) and Crosby et al. (1993).

Alternatively to the chosen method of least-square fitting of differential or cumulative size distributions, other methods have been used to test the consistency of an ideal power law function with observed size distributions, such as the maximum likelihood estimator, the Bayesian information criterion, the Anderson-Darling test, or the Kolmogorov-Smirnov statistic (Clauset et al. 2009). However, since no accomodation for (i) undersampling of small events, (ii) subtraction of event-unrelated background, or (iii) automated determination of a threshold is provided in those alternative methods, they are not suitable for modeling of astrophysical data (Aschwanden 2015).

2.3. Solar Flare Observations

The results of the data analysis are presented in Figs. (2-6) and in Table 1. While we used the generic term “size” in the definition of occurrence frequency distributions, we should be aware that the size can be represented by any measure, magnitude, or physical quantity that can be measured in a set of events, but we should not expect to find the same power law slope for different quantities, because there is often some nonlinear scaling involved. For the solar observations analyzed here we sample the following quantities: peak count rates of the hard X-ray photon fluxes of flares (P) (observed with the instruments HXRBS, the *Burst and Transient Source Experiment (BATSE)* on the *Compton Gamma Ray Observatory (CGRO)*, and the *Ramaty High Energy Solar Spectroscopic Imager (RHESSI)* spacecraft), total counts (or fluences) of hard X-ray fluxes (C), flare durations (T), emission measure (EM) in soft X-rays and EUV, thermal flare energies (E_{th}), nonthermal flare energies (E_{nth}), dissipated magnetic energies (E_{mag}), flare volumes (V), flare areas (A), and flare length scales (L). The energetic parameters have been calculated in recent statistical studies on the global energetics of solar flares (Aschwanden et al. 2014, 2015, 2016).

The results of forward-fitting differential and cumulative size distributions of different events are summarized in Table 1, which includes: background counts (BG), the number of all events (N), the number of events above threshold (NT), the logarithm of the inertial range $\log(x_2/x_1)$ (IR), the threshold value (x_0), the power law slope from fitting differential (α_{diff}) and cumulative occurrence frequency distributions (α_{cum}), the χ^2 -values of differential (χ_{diff}) and cumulative size distributions (χ_{cum}), and the mean χ^2 -values in the range of the 10 most extreme events (χ_{ee}).

We determined the background level by minimizing the goodness-of-fit χ^2 -criterion as a function of the background level (see Fig. 7 in Aschwanden et al. 2015). It turned out that only the HXRBS data needed background subtraction (by 41 and 58 cts s⁻¹), while the BATSE and RHESSI flare catalogs provide background-subtracted flux values.

The total number of events (N in Table 1) encompasses all sampled events, but only those (NT) above the threshold x_0 could be used in the fitting of size distributions. The inertial range is characterized by the logarithmic ratio $\log(x_2/x_0)$, which ranges from 2 to 5 decades. Those with the largest inertial ranges and largest number of events provide the most accurate fits of size distributions.

2.4. Self-Consistency of Size Distributions

A first important test is the self-consistency between the two different methods, i.e., the fitting of the differential and cumulative size distributions. We can simply compare the resulting power law slopes, which are labeled as α_{diff} and α_{cum} in Table 1. We find a satisfactory agreement between the two methods within the derived uncertainties of a few percents, as it can be seen for all data sets with large statistics (Table 1: $N \approx 10^3 - 10^4$ events). This corroborates the self-consistency between the two methods. The high accuracy is mostly achieved by modeling the size distribution with a thresholded power law distribution function (Eqs. 3 and 6), which is more suitable to represent the data than an ideal power law function.

A second important test is the comparison of the goodness-of-fit between the differential and cumulative size distributions, labeled as χ_{diff} and χ_{cum} in Table 1. Among the 9 fitted size distributions of 3 solar observables (P, C, T) with 3 different instruments each (HXRBS, BATSE, RHESSI), shown in Fig. 2, we find that only one data set is consistent with the fitted (differential and cumulative) size distributions, namely P of HXRBS, with $\chi_{diff} \approx 2$ and $\chi_{cum} \lesssim 2$, while the other 8 data sets exhibit significant mismatches $\chi_{diff} \approx \chi_{cum} \approx 3 - 13$. This indicates that the large number statistics of these data sets is sensitive to apparently little but significant deviations from power laws. These deviations can clearly be recognized in the poor values $\chi_{diff,all}$ and $\chi_{cum,all}$ in the plots of Figs. (2b-2i). There is a tendency that peak count (P) size distributions match a power law function closest, while the total counts (C) and the flare durations (T) deviate significantly. The reason for the latter property could be due to a violation of the principle of time scale separation that is required in SOC models (Aschwanden et al. 2016), caused by confusion between overlapping short and long-duration flares.

2.5. Energetic Solar Flare Parameters

The flare observables (P, C, T) are easiest to measure and have often been used in modeling of SOC models. However, since these observables may not be a good proxy for the representation of the energy contained in SOC avalanches, we inspect also the size distribution of spatial and flare parameters, such as ($L, A, V, E_{mag}, E_{th}, E_{nth}, EM$), which have been determined under the scope of global energetics in solar flares in a series of ongoing studies (Aschwanden et al. 2014, 2015, 2016). The cumulative size distributions are presented in Figs. 3 and 4. Since the number of events, for which energetic parameters have been determined, includes M and X GOES-class flares only, we deal with small-number statistics in the order of $N \approx 100 - 300$ events per data set. Consequently, the resulting fits yield acceptable values for the goodness-of-fit, i.e., $\chi^2 \lesssim 2$, but these small data sets have insufficient sensitivity to measure deviations from power law functions. Nevertheless, since they contain large flares only, they are suitable to detect the outliers of extreme events.

The only obvious deviation from a power law is detected for the size distribution of nonthermal energies (Fig. 4b), which is suspected to arise due to an instrumental irregularity, such as pulse pile-up in RHESSI data.

2.6. Extreme Events

We investigate now the so-called Dragon-King hypothesis (Sornette 2009; Sornette and Ouillon 2012). This hypothesis suggests that the most extreme events may belong to a different population of event size distributions than smaller or even large events. In this study we define three different parameters to characterize Dragon-King events: (i) A range of largest extreme events in a data set, which we set arbitrarily to $n_{ee} = 10$ here; (ii) The ratio of the observed size $x_{max,obs} = x_2$ to the expected size $x_{max,fit}$ of the most extreme event, based on the cumulative size distribution fit, i.e., $q_{ee} = x_{max,obs}/x_{max,fit}$, (which we may call the *extreme event excess factor*), and (iii) the goodness-of-fit χ_{ee} of the cumulative size distribution fit in the range of the largest $n_{ee} = 10$ events. These three values are given in the lower right corner of each panel in Figs. 1-6 and Table 1.

As an example we consider Fig. 1, where the goodness-of-fit in the extreme event part of the size distribution, i.e., $\chi_{ee} = 0.56$, which compares well with the value obtained from fitting all events above the threshold, i.e., $\chi_{all} = 1.46$, which does not yield any evidence for a different population. A second test is the extreme event excess factor, which for this event is $q_{ee} = 1.03$ and yields no evidence for a Dragon-King event either (Fig. 1c).

We list all evaluated extreme event excess factors q_{ee} in Table 1 (also given in the panels of Figs. 1-6). Among the solar flare parameters, all those factors vary in the range of $q_{ee} \approx 0.9 - 1.9$, with a single outlier of $q_{ee} = 3.08$ (for one flare volume data set, see Fig. 3c), out of 23 solar data sets. Therefore, we see no indication that solar extreme events belong to different populations of event distributions.

The estimation of an unknown tail distribution function can be derived with tools from *extreme value theory*, such as with the *Pickands-Balkema-de Haan theorem* (Balkema and de Haan 1974; Pickands 1975), the *Fisher-Tippett-Gnedenko theorem* (Fisher 1930), or as described in Gumbel (1958), which converge to three possible distributions (the Gumbel distribution, the Fréchet distribution, or the Weibull distribution). In our case, however, the cumulative form of the *thresholded power law size distribution* (generalized Pareto) function is our preferred model of choice, due to its ability of taking incomplete sampling, background subtraction, and finite system size into account, and thus is known a priori, so that it does not need to be estimated with extreme value theory, as it would be needed in the case of an unknown tail distribution function. The theoretically defined distribution is then fitted to the observed distributions directly, and the *extreme event excess factor* q_{ee} is conveniently quantified in terms of standard deviations in common χ^2 -statistics.

2.7. Stellar Flare Observations

Impulsive flaring with rapid increases in the brightness in UV or EUV has been observed for a number of so-called flare stars, such as AD Leo, AB Dor, YZ Cmi, EK Dra, or ϵ Eri. These types of stars include cool M dwarfs, brown dwarfs, A-type stars, giants, and binaries in the Hertzsprung-Russell diagram. Most of these stars are believed to have hot soft X-ray emitting coronae, similar to our Sun (a G5 star), and thus magnetic reconnection processes are believed to operate in a similar way as on our Sun (see, e.g., review by Güdel 2004).

We complement the solar flare data sets with three data sets of stellar flares, two recorded with KEPLER and one observed with the EUVE telescope, with the cumulative size distributions shown in Figs. (4g, 4h) and Fig. (5). The fit of a cumulative power law distribution shown in Fig. (4g) produces a size distribution

with a power law slope of $\alpha = 1.68 \pm 0.12$ for the peak counts, which is similar to the slope observed in solar flares, i.e., $\alpha = 1.70 \pm 0.02$ with HXRBS (Fig. 2a), $\alpha = 1.81 \pm 0.02$ with BATSE (Fig. 2b), and $\alpha = 1.86 \pm 0.02$ with RHESSI (Fig. 2c). The goodness-of-fit for extreme events is $\chi_{ee} = 1.45$, which is similar to $\chi_{all} = 1.26$ for all events (Fig. 4g).

A second data set with stellar flare data from KEPLER, derived from the bolometric energy, is shown in Fig. (4h), yielding a power law slope of $\alpha_{bol} = 2.55 \pm 0.06$, which is similar to the value expected for flare areas $\alpha_A = 2.33$ (Table 2). Since the largest contributions to the bolometric intensity come from the solar or stellar photospheric surface area, it makes sense the its size distribution scales with the flare area (rather than with a 3-D volume).

In Fig. 5 we present cumulative size distribution fits of 12 cool (type F to M) stars, observed by Audard et al. (2000), with typically 5-15 flare events per star. For most of these stars, the flare intensities follow closely the fitted cumulative distribution all the way to the most extreme event, except for two cases (out of 12): HD 2726 (F2 V) (top left panel) and CN Leo, 1994 (M6 V) (bottom middle panel), which could qualify as outliers (or Dragon-King events). The power law slopes inferred in this sample vary strongly within a range of $\alpha \approx 2.0 \pm 0.4$, which tend to be somewhat higher than the mean values of solar flare size distributions, but are not reliable in such small number statistics.

In summary, stellar flares fit cumulative size distributions at the upper cutoff (within an energy range of $\approx 0.8 - 1.4$ decades), but the power law slopes appear to be slightly steeper than observed in solar flares, and outliers of extreme events occur only rarely (in 2 out of 12 cases).

3. DISCUSSION

3.1. Astrophysical Predictions of Power Law Slopes

While we are interested in the investigation of deviations from ideal power laws, which is a second-order effect, we should consider first the physical justification of the existence of power law size distributions in the first place. The original discoverers of *self-organized criticality* (SOC) models noted power law-like size distributions with power law slopes of $\alpha_x \approx 2$ of the sizes x of SOC avalanches, as well as power law slopes of $\alpha_T \approx 2$ for the durations T of SOC avalanches, obtained in cellular automaton simulations (e.g., Pruessner 2012). A more physical approach of modeling and predicting power law slopes of size distributions observed from astrophysical SOC systems has been put forward in terms of the so-called *Fractal-Diffusive* (FD-SOC) model (Aschwanden 2013, 2014, 2016). We juxtapose theoretical predictions of this model and mean observational values in Table 2.

The most fundamental assumption in the FD-SOC model is the *scale-free probability conjecture*, which directly predicts a power law size distribution function of geometric length scales L from first principles, i.e.,

$$N(L)dL = L^{-S} dL , \quad (15)$$

where S is defined as the Euclidean dimension of the SOC system (with possible values of $S = 1, 2, 3$). From this fundamental power law distribution, other power law size distributions of any physical size parameter x that has a linear ($x \propto L$), or a nonlinear relationship $x(L) \propto L^p$ to the length scale L (with power index p), can be derived. The following scaling laws have been used in the calculation of the power law indices listed in Table 2:

$$A \propto L^{D_2} \quad (16)$$

$$V \propto L^{D_3} \quad (17)$$

$$L \propto T^{\beta/2} \quad (18)$$

$$F \propto V^\gamma \propto L^{D_S \gamma} \quad (19)$$

$$P = F_{max} \propto V_{max}^\gamma \propto L^{S\gamma} \quad (20)$$

$$E = F T \propto L^{(\gamma D_S + 2/\beta)} \quad (21)$$

where D_2 is the area (A) fractal dimension, D_3 is the volume (V) fractal dimension, β is the spatio-temporal diffusion coefficient for the time duration (T) of a SOC avalanche with classical diffusion ($\beta = 1$), γ is the flux-volume scaling of observed fluxes F of astrophysical sources, V_{max} is the maximum fractal volume, which obeys the Euclidean dimension S of the SOC system, $P = F_{max}$ is the peak or maximum flux, and $E = F T$ is the fluence, defined as the product of the flux F and time duration T .

The mean fractal dimension is estimated from the average of the minimum ($D_{S,min} \approx 1$) and maximum $D_{S,max} = S$ values,

$$D_S \approx \frac{(D_{S,min} + D_{S,max})}{2} = \frac{(1 + S)}{2}, \quad (22)$$

which yields $D_2 = (1 + 2)/2 = 3/2$ and $D_3 = (1 + 3)/2 = 2$ for SOC models that occupy either an Euclidean 2-D or 3-D dimensional space.

Since all relationships given in Eq. (15-21) are expressed in terms of the variable L , the power law indices α_x for the size distribution of the parameters $x = A, V, T, F, P, E$ can be derived by substitution of variables, i.e., $N(x)dx = N[x(L)] |dx/dL| dL \propto x^{-\alpha_x}$, yielding the power law indexes α_x ,

$$\alpha_L = S \approx 3 \quad (23)$$

$$\alpha_A = 1 + (S - 1)/D_2 \approx 7/3 \quad (24)$$

$$\alpha_V = 1 + (S - 1)/D_3 \approx 2 \quad (25)$$

$$\alpha_T = 1 + (S - 1)\beta/2 \approx 2 \quad (26)$$

$$\alpha_F = 1 + (S - 1)/(\gamma D_S) \approx 2 \quad (27)$$

$$\alpha_P = 1 + (S - 1)/(\gamma S) \approx 5/3 \quad (28)$$

$$\alpha_E = 1 + (S - 1)/(\gamma D_S + 2/\beta) \approx 3/2, \quad (29)$$

where the approximative numerical values are obtained by inserting $S = 3, \beta = 1, \gamma = 1, D_2 = 1.5, D_3 = 2$.

In Table 2 we juxtapose these theoretical power law slope values with the observed values. We see that there is mostly a good agreement (within a few percents) for solar flare size distributions with large statistics ($N \approx 10^3 - 10^4$), such as for peak fluxes (α_P), total counts (α_C), and flare durations (α_T), while others with small number statistics show larger deviations from the predictions, such as for length scales (α_L), areas (α_A), and volumes (α_V).

New results are obtained here from the power law slopes of energetic flare parameters. The dissipated magnetic energies E_{mag} are found to have power law indices that are close to the values of flare areas, i.e., $\alpha_{mag} = 2.8 \pm 0.2$ versus $\alpha_A \approx 2.3$, which could be explained by the fact that the dissipation of free magnetic energies is concentrated in the chromospheric flare ribbons, which have a horizontal area-like surface geometry. This is also true for the bolometric flare energies observed in stellar flares, i.e., $\alpha_{bol} = 2.6 \pm 1.0$ versus $\alpha_A \approx 2.3$, since the bolometric brightness is mostly irradiated in the photosphere of stellar surfaces. Also for the thermal emission measure we find similarity with area-like features, i.e., $\alpha_{EM} = 2.8 \pm 0.2$ versus $\alpha_A \approx 2.3$, which suggests that the soft X-ray emission measure in solar flares has an area-like extension with

relatively low altitudes. For thermal flare energies, for which we expect mostly a volume dependence,

$$E_{th} = 2n_e k_B T_e V \propto V \propto L^{D_3}, \quad (30)$$

since the electron density and the electron temperature vary much less than the flare volume. Indeed we find values of $\alpha_{E_{th}} = 2.2 \pm 0.1$ that are similar to the volume power law index, $\alpha_V \approx 2$. For nonthermal flare energies we find a close coincidence of the power law slope of $\alpha_{E_{nth}} = 1.57 \pm 0.11$, which is close to the power law slopes of fluences, $\alpha_C \approx 1.50$, which is expected because both the fluences ($E = F T$) and the nonthermal energies, $E_{nth} = \int e_{nth}(t) dt$, are time-integrated flare quantities.

These comparisons of power law indices thus reveal interesting relationships that are relevant for determining the physical scaling laws that govern solar flares.

3.2. Outliers or Dragon-King Events

From the 23 solar (Figs. 3, 4) and 14 stellar data sets (Figs. 4, 5) we found little evidence for outliers among the most extreme events in each data set. The largest outliers for the most extreme events are found for a small data set ($N = 172$) of flare volumes with an excessive extreme event factor of $q_{ee} = 2.75$ (Fig. 3c), for a small stellar flare data set ($N = 209$) with $q_{ee} = 3.55$ (Figs. 4g), and for the two stars HD 2726 and CN Leo with even less statistics ($N \approx 15$) (Fig. 5). The fact that all these most extreme events occur in small data sets, while larger data sets with $N \gtrsim 10^3 - 10^4$ events (Fig. 2) reveal no excesses larger than $q_{ee} \lesssim 2.0$, provides little evidence for the existence of super-extreme events that are not part of the “normal” population of small and large flare events. Hence, we conclude that extreme events of solar and stellar flares are largely scale-free (over an inertial range of $\approx 3 - 4$ decades) in their volumes, fluxes, or energies.

What does it mean that we find no significant outliers in the cumulative size distributions of solar and stellar flares? As the size distribution of length scales reveals in Fig. (3a), solar flares have length scales of $L \approx 10 - 200$ Mm, which at the upper limit matches the maximum size of active regions on the solar surface. The largest possible flare that extends over the entire solar surface would have a circumference of $2\pi \times 696$ Mm, which is apparently impossible since we never observed a flare with a size larger than $L \lesssim 200$ Mm. One effect that could help to increase the maximum flare size is the case of *sympathetic flaring*, which involves a magnetic coupling between adjacent (or even remote) active regions. However, the larger an unstable magnetic field configuration is, the smaller is the filling factor of magnetic energy and heated plasma with respect to the size of a flaring region. Consequently, the envisioned process of amplification and synchronization promoted in the Dragon-King hypothesis (Sornette 2009; Sornette and Ouillon 2012) seems to be questionable for solar and stellar flares.

3.3. Deviations from Power Laws

It has been argued that real data deviate from ideal power law size distributions, as they have been reproduced by cellular automaton simulations (e.g., Pruessner 2012). Some sceptics went even as far as to deny the existence of power laws at all (Stumpf and Porter 2012). Traditional least-square fitting techniques have been criticized to be inaccurate, while maximum-likelihood fitting methods with goodness-of-fit tests based on the Kolmogorov-Smirnov statistic were preferred (Clauset et al. 2009). However, we have demonstrated here and earlier (Aschwanden 2015) that least-square fitting methods of both differential and cumulative size distributions yield self-consistent fits of the power law slope, as long as data truncation, undersampling

of data in small events below some threshold, subtraction of event-unrelated background noise, and the steep fall-off at the upper bound of the cumulative size distribution is properly modeled. In other words, a straight power law function represents an over-simplified model for most cases, while inclusion of the effects enumerated above is essential in defining adequate models for fitting statistical distributions.

Now, with the availability of large data sets (with $N \approx 10^5 - 10^8$ events), we are becoming much more sensitive to the smallest deviations from ideal power laws. So it is no surprise that deviations from power laws become the rule rather than the exception. The deeper reason for these power law deviations is the inhomogeneity of the medium and the physical conditions. It is instructive to consider the sandpile analogy of SOC systems. Although the cone shape of a sandpile appears to have a constant slope or angle of repose, when viewed from distance, closer inspection reveals macroscopic channels, erosions, bumps, and dents, on top of the microscopic fine structure. As an illustration we mention some empirical data sets (chosen by Clauset et al. 2009) that are shown in Fig. 6 and described in Appendix A. Some data sets clearly reveal a complete inadequacy to fit any power law function to data with a broken power law (Fig. 6b: wildfires; Fig. 6c: cities). The case of weblinks has such a tremendous statistic ($N = 1.35 \times 10^8$ events) that it is highly sensitive to the smallest deformations from an ideal power law, i.e., amounting to $\chi_{all} = 223$ for a slight deficit near $x \approx 10^5 - 10^6$ (Fig. 6h). A Dragon-King event with an excess of $q_{ee} \approx 5$ is indicated in the data set of terrorism (Fig. 6e).

Significant deviations from ideal power law size distributions have also been detected in stellar flares, e.g. in the Kepler-based study of Sheikh et al. (2016), and most of the analyzed stars were found to exhibit no evidence for SOC avalanching. It is argued that these stellar flares are subject to “tuned criticality” rather than “self-organized criticality” (Sheikh et al. 2016).

3.4. Physical Mechanisms of SOC Avalanches

The observations of SOC avalanches exhibit power law-like size distributions, which constrain (scale-free) scaling laws of physical parameters (see Section 3.1), but do not directly reveal the physical mechanism of SOC processes as such. The power law slopes of the size distributions of solar and flare data have been found to be consistent with the scale-free probability conjecture (Eq. 15), fractal-diffusive transport (Eq. 18), and with EUV and soft X-ray emission (flux or intensity) that is quasi-proportional to the fractal volume of an avalanche event (Eq. 20). These scaling laws are consistent with standard solar flare models, which are driven by a magnetic reconnection process in the solar corona (Lu and Hamilton 1991). However, the observed scaling laws are also consistent with other physical mechanisms, such as turbulent photospheric convection, which may be (stochastically) coupled with coronal reconnection events (Uritsky et al. 2013; Uritsky and Davila 2012; Knizhnik et al. 2017). Additional interpretations of physical mechanisms operating in SOC systems can be found in Aschwanden et al. (2011, 2016).

The interpretation of SOC systems in terms of physical mechanisms is beyond the scope of this study, but the fact that we find virtually no outliers or Dragon-King events implies that only one single physical mechanism with appropriate properties is needed to explain the observed power law size distributions. A dual energy dissipation system is likely to produce broken power law distributions. However, the same physical process, such as a magnetic reconnection process, can have multiple secondary energy dissipation processes, including nonthermal particle acceleration (hard X-ray fluxes), thermal flare plasma heating (soft X-ray fluxes), launching of a coronal mass ejection (white light emission), or electron beam formation (radio emission). Quantitative energy budget calculations have revealed energy closure for the primary flare-

dissipated magnetic energy and secondary energy dissipation mechanisms (Aschwanden et al. 2017). All energy that is dissipated during a solar flare is supplied by the free (magnetic) energy in an active region. Interestingly, multi-scale intermittent dissipation with power law-like SOC properties has also been detected in Quiet Sun regions at spatial scales of $\gtrsim 3$ Mm, controlled by turbulent photospheric convection (Uritsky et al. 2013). It appears that we observe a coexistence of coronal SOC systems (in active regions) and photospheric SOC systems (in Quiet Sun regions).

4. CONCLUSIONS

In this study we search for outlier events in astrophysical data sets from solar and stellar flares. Such an endeavour is motivated by the “*Dragon-King hypothesis*” (Sornette 2009; Sornette and Ouillon 2012), which suggests that the most extreme events in a statistical distribution may belong to a different population, and thus may be generated by a different physical mechanism, than the ubiquitous power law distributions commonly observed in nonlinear systems driven by self-organized criticality. For this project we extracted 23 data sets of solar flare data (from HXRBS/SMM, BATSE/CGRO, RHESSI, AIA/SDO, HMI/SDO), 12 data sets from stellar flares (from EUVE and KEPLER), and another 8 data sets of non-astrophysical data. We define a thresholded power law distribution, which includes the effects of data truncation, undersampling of small events below a threshold, subtraction of event-unrelated background noise, and the steep fall-off at the upper bound of cumulative size distributions. We tested the accuracy of our size distribution forward-fitting method for both the differential and the cumulative occurrence frequency size distributions, as well as using the method of rank-order plots. Our least-square fitting techniques focus mostly on detecting deviations from ideal power laws (by means of the χ^2 -criterion) and on detecting outliers of the most extreme events in each statistical distribution. In the following we summarize the major conclusions.

1. *Identifying Dragon-King events is important for accurate predictions and forecasting of the largest catastrophes.* For solar and stellar flare data, the frequency and size of the most extreme events have generally been established from extrapolating power law distributions, which may under-estimate the largest events, if such outlier events belong to a different population and are generated by different physical mechanisms. Prediction and forecasting of large events generated by solar flares or coronal mass ejections have been recognized to play a central role in *space weather predictions* (e.g., Schrijver 2007, 2009; Gallagher et al. 2002; Georgoulis and Rust 2007; Leka and Barnes 2007; Barnes et al. 2007; Barnes and Leka 2008; Bloomfield et al. 2002; Aschwanden 2019, Section 16.8 and 16.9 and references therein).
2. *Dragon-King events are theoretically possible in solar and stellar flares*, e.g., in the case of sympathetic flaring. Sympathetic flares are a pair of flares that occur almost simultaneously in different active regions, not by chance, but because of some physical connection (for instance by propagating Alfvénic waves). Statistical evidence for sympathetic flaring has been established for 48 events, some of them consisting of trans-equatorial loops (Moon et al. 2002). Another example is a quadrupolar configuration with two magnetic flux ropes that are located within a pseudo-streamer, which have been observed to lead to two consecutive reconnections and eruptions, a scenario for twin-filament eruptions that can explain coupled sympathetic eruptions also (Török et al. 2011). Coupling flares in adjacent regions could double up the joint flare volumes and energies, if both active regions have similar sizes.
3. *Dragon-King events are not common in solar and stellar flares.* In our analysis we measured excessive extreme event factors q_{ee} for each data set, which characterizes the offset of outliers by the ratio of the

observed most extreme event to the expected most extreme size based on a cumulative size distribution fit. We found that this factor amounts generally to less than a factor of $q_{ee} \lesssim 2$, in 21 out of the 25 investigated solar and stellar size distributions. The four cases possibly containing Dragon-King events were found for solar flare volumes ($q_{ee} = 3.08$), stellar flare peak counts ($q_{ee} = 3.55$), and in flares from the red dwarf stars HD 2726 and AD Leo (Fig. 5). However, Dragon-King events have been found in other, non-astronomical data sets (Fig. 6), such as in earthquakes ($q_{ee} = 2.82$), power blackouts ($q_{ee} = 3.35$), and terrorism ($q_{ee} = 6.15$).

4. *Extreme events of solar and stellar flares are scale-free.* The fact that almost all extreme events of solar and stellar flares fit a power law size distribution with a small value of the excessive extreme event factor ($q_{ee} \lesssim 1.5$) indicates that solar and stellar flare processes are scale-free (within the inertial range), and thus can be modeled with the same power law (SOC) model for small or large events. This implies also that small and large flare events are subject to the same physical mechanism, most likely caused by a magnetic reconnection process in active regions, driven by shearing and twisting of the magnetic field.
5. *Deviations from power laws are common in large-number statistical distributions.* Adversely, distributions with acceptable power law fits are more likely to be found in size distributions with small-number statistics. The accuracy of fitting power law slopes scales with the square root of the number of events, and hence the measurement of deviations from ideal power laws is a matter of instrumental sensitivity. However, large-number statistics ($N \gtrsim 10^4$) requires comprehensive flare catalogs or automated pattern recognition codes, which is the reason why we have a high accuracy of power law fits for extensive data sets only, such as for peak counts (P), total counts (C), or time durations (T), while energetic parameters could only be measured in large (GOES M and X-class) flares, yielding small-number statistics ($N \gtrsim 10^2$) with a lower degree of accuracy.
6. *Accurate size distributions provide tests of physical scaling laws in solar and stellar flares.* The fractal-diffusive SOC model predicts a set of power law slopes (for avalanches in a SOC system) that can straightforwardly be compared with the corresponding observed size distributions. Consequently, the obtained power law slopes provide consistency tests of the underlying physical scaling laws. In this study we discovered new correlations that indicate that the dissipated magnetic energies ($\alpha_{mag} \propto \alpha_A$), flare emission measures ($\alpha_{EM} \propto \alpha_A$), and bolometric energies ($\alpha_{bol} \propto \alpha_A$) scale with the flare area, that the thermal flare energy scales with the flare volume ($\alpha_{th} \propto \alpha_V$), and that the nonthermal energy scales with the total (time-integrated) hard X-ray counts ($\alpha_{nth} \propto \alpha_C$). The reason why these flare scaling laws can be inferred mostly from the flare volume V or area A is the high nonlinearity of these geometric parameters ($V \propto L^3$, $A \propto L^2$), while other physical parameters (such as the electron density n_e or temperature T_e) scale only linearly in the definitions of the thermal energy and pressure.

There are a lot of new questions that arise from this study that can be addressed in follow-on work: What physical conditions are different in Dragon-King events? Does sympathetic flaring occur in the most extreme events? Which stars produce outliers and what is different in the flare productivity of these stars? If we increase the size of the data sets to large-number statistics, do we obtain more accurate power law slopes that converge from different instruments? If we improve the statistics, do the power law indices in physical scaling laws converge to the theoretically predicted values? Can stellar power laws be used to tell us which flare phenomena are controlled by the flare size and their relationship to the depth of the stellar convection zone?

APPENDIX A: Empirical Data

In the spirit of interdisciplinary research, let us visit eight non-astrophysical data sets of empirical data (Fig. 6, Table 1), which have been compiled and scrutinized for deviations from ideal power laws by Clauset et al. (2009). If we investigate the goodness-of-fit χ^2 -values of all events in each data set, we find significant deviations from ideal power laws for most of the cases, except for blackouts (Fig. 6e: $\chi_{cum} = 0.83$), but this phenomenon has also the smallest statistics ($N = 210$), and thus is not sensitive to small deviations from power laws. On the other hand, if we consider just the average goodness-of-fit χ^2 -values among the 10 most extreme events, we find consistency with thresholded power law distributions for earthquakes (Fig. 6a: $\chi_{ee} = 1.45$), blackouts (Fig. 6d: $\chi_{ee} = 0.63$), terrorism (Fig. 6d: $\chi_{ee} = 0.43$), surnames (Fig. 6g: $\chi_{ee} = 1.34$), and weblinks (Fig. 6h: $\chi_{ee} = 1.07$). These results differ somewhat from those obtained in Clauset et al. (2009), although they also find most of the data are not consistent with an ideal power law distribution, which is expected for fitting different functions to the observed distributions, such as the thresholded Pareto-type power law function used here. The evaluation of power law deviations in Clauset et al. (2009) is subject to an arbitrary truncation of small events, while our method derives a threshold automatically, which is important, because the choice of (scale-free) inertial range boundaries affects the outcome of the power law slope value most.

Acknowledgements: This work was stimulated by the organizers of a workshop on “*Mechanisms for extreme event generation*” (*MEEG*) at the Lorentz Center at Snellius, Leiden, The Netherlands, July 8-12, 2019, organized by Drs. Norma Bock Crosby, Bertrand Gros Lambert, Alexander Milovanov, Jens Juul Rasmussen, and Didier Sornette. The author acknowledges the hospitality and partial support of two previous workshops on “Self-Organized Criticality and Turbulence” at the *International Space Science Institute (ISSI)* at Bern, Switzerland, during October 15-19, 2012, and September 16-20, 2013, as well as constructive and stimulating discussions with Sandra Chapman, Paul Charbonneau, Aaron Clauset, Norma Crosby, Michaila Dimitropoulou, Manolis Georgoulis, Stefan Hergarten, Henrik Jeldtoft Jensen, James McAteer, Shin Mineshige, Laura Morales, Mark Newman, Naoto Nishizuka, Gunnar Pruessner, John Rundle, Surja Sharma, Antoine Strugarek, Vadim Uritsky, and Nick Watkins. This work was partially supported by NASA contracts NNX11A099G “Self-organized criticality in solar physics”, NNG04EA00C of the SDO/AIA instrument, and NNG09FA40C of the IRIS instrument.

References

- Aschwanden, M.J.: 2004, *Physics of the Solar Corona. An Introduction*, Berlin: Springer and Praxis, p.216.
- Aschwanden, M.J. 2011, *Self-Organized Criticality in Astrophysics. The Statistics of Nonlinear Processes in the Universe*, Springer-Praxis: New York, 416p.
- Aschwanden, M.J., Xu, Y., and Jing, J. 2014, ApJ 797:50.
- Aschwanden, M.J., Boerner, P., Ryan, D., Caspi, A., McTiernan, J.M., and Warren, H.P. 2015, ApJ 802:53.
- Aschwanden, M.J. 2015, ApJ 814:19.
- Aschwanden, M.J. (ed.) 2013, *Self-Organized Criticality Systems*, Open Academic Press, Berlin, Warsaw, 483p.
- Aschwanden, M.J., Crosby, N., Dimitropoulou, M., Georgoulis, M.K., Hergarten, S., McAteer, J., Milovanov, A., Mineshige, S., Morales, L., Nishizuka, N., Pruessner, G., Sanchez, R., Sharma, S., Strugarek, A., and Uritsky, V. 2016, SSRv 198, 47.
- Aschwanden, M.J., Caspi, A., Cohen, C.M.S., Holmen, G., Jing, J., Kretzschmar, M., Konter, E.P., McTiernan, J.M. 2017, ApJ 836, 17.
- Aschwanden, M.J. 2019, *New Millennium Solar Physics*, Astrophysics and Space Science Library, Volume 458, ISBN 978-3-030-13954-4, Springer Nature Switzerland AG; DOI: 10.1007/978-3-030-13956-8, (Section 11.8).
- Audard M., Güdel, M., Drake, J.J., and Kashyap V.I. 2000, ApJ 541, 396.
- Bak, P. 1996, *How nature works : the science of self-organized criticality*, Copernicus, New York.
- Balkema, A. and de Haan L. 1974, Annals of Statistics 2, 792.
- Balona, L.A. 2015, MNRAS 447, 2714.
- Barnes, G., Leka, K.D., Schumer, E.A., et al. 2007, Space Weather 5/9, S09002.
- Barnes, G. and Leka, K.D. 2008, ApJ 688, L107.
- Baro, J., Corral, A., Illa, X., Planes, A., Salje, E.K.H., Schranz, W., Soto-Parra, D., and Vives, E. 2013, Phys. Rev. Lett. 110, 088702.
- Bloomfield, D.S., Higgins, P.A., McAteer, R.T.J., et al. 2012, ApJ 747, L41.
- Charbonneau, P., McIntosh, S.W., Liu, H.L., and Bogdan, T.J. 2001, SoPh 203, 321.
- Clauset, A., Shalizi, C.R., and Newman, M.E.J. 2009, SIAM Rev. 51/4, 661.
- Crosby, N.B., Aschwanden, M.J., and Dennis, B.R. 1993, SoPh 143, 275.
- Dennis, B.R. 1985, SoPh 100, 465.
- Fisher, R.A. 1930, *The Genetical Theory of Natural Selection*, Oxford University Press, Oxford.
- Gallagher, P.T., Moon, Y.J., and Wang, H. 2002, SoPh 209, 171.
- Georgoulis, M.K. and Rust, D.M. 2007, ApJ 661, L109.

- Güdel, M. 2004, *Astron. Astrophys. Rev.* 12(2-3), 71.
- Gumbel, E.J. 1958, *Statistics of extremes*, Columbia University Press, Hew York.
- Hergarten, S. 2002, *Self-Organized Criticality in Earth Systems*, Springer, Berlin.
- Hosking, J.R.M. and Wallis, J.R. 1987, *Technometrics* 29, 339.
- Jensen, H.J. 1998, *Self-Organized Criticality: Emergent complex behaviour in physical and biological systems*, Cambridge University Press.
- Knizhnik, K.J., Uritsky, V.M., Klimchuk, J.A., and DeVore, C.R. 2018, *ApJ* 853, 82.
- Leka, K.D. and Barnes, G. 2003, *ApJ* 595, 1277.
- Lomax, K.S. 1954, *J. Am. Stat. Assoc.* 49, 847.
- Lu, E.T., and Hamilton, R.J. 1991, *ApJ* 380, L89.
- Moon, Y.J., Choe, G.S., Park, Y.D., Wang, H., Gallagher, P.T., Chae, J., Yun, H.S., and Goode, P.R. 2002, *ApJ* 574, 434.
- Pickands, J. 1975, *Annals of Statistics* 3, 119.
- Pruessner, G. 2012, *Self-organised criticality. Theory, models and characterisation*, Cambridge University Press, Cambridge.
- Schrijver, C.J. 2007, *ApJ* 655, L117.
- Schrijver, C.J. 2009, *AdvSpR* 43, 739.
- Sharma, A.S. 2017, *Data-driven modeling of extreme space weather*, in *Extreme Events in Geospace* (ed. Buzulukova, N.), Elsevier.
- Sharma, A.S., Aschwanden, M.J., Crosby, N.B., Klimas, A.J., Milovanov, A.V., Morales, L., Sanchez, R., and Uritsky, V., 2016, *SSRv* 168, 167.
- Sheikh, M.A., Weaver, R.L., and Dahmen, K.A. 2016, *Phys.Rev.Lett.* 117/26, id. 26110.
- Sornette, D. 2004, *Critical phenomena in natural sciences: chaos, fractals, selforganization and disorder: concepts and tools*, Springer, Heidelberg.
- Sornette, D. 2009, *J. Terraspace Science and Engeneering*, 2(1), 1.
- Sornette, D. and Ouillon, G. 2012, in *The European Physical Journal Special Topics “Discussion and Debate: From Black Swans to Dragon-Kings – Is There Life Beyond Power Laws?*, 205, 1.
- Stumpf, M.P.H. and Porter, M.A. 2012, *Science* 335, 6069.
- Török, T., Panasenco, O., Titov, V.S., Mikic, Z., Reeves, K.K., Velli, M., Linker, J.A., and De Toma G. 2011, *ApJ* 739, L63.
- Uritsky, V.M., Davila, J.M., Ofman, L., and Coyner, A.J. 2013, *ApJ* 769, 62.
- Uritsky, V.M. and Davila, J.M. 2012, *ApJ* 748, 60.
- Watkins, N.W., Pruessner, G., Chapman, S.C., Crosby, N.B., and Jensen, H.J. 2016, *SSRv* 198, 3.

Table 1: Results of forward-fitting of differential and cumulative size distributions for different statistical events, characterized by background counts (BG), the number of all events (N), the number of events above threshold (NT), the inertial range $\log(x_2/x_1)$ (IR), the threshold value (x_0), the power law slope from fitting a differential size distribution α_{diff} , the power law slope from fitting a cumulative size distribution α_{cum} , the goodness-of-fit values for both types of fits (χ_{diff}, χ_{cum}), restricted to the range of the 10 most extreme events (χ_{ee}), and the excessive extreme event factor (q_{ee}).

	BG	N	NT	IR	x_0	α_{diff}	α_{cum}	χ_{diff}	χ_{cum}	χ_{ee}	q_{ee}
<u>Solar flares:</u>											
Peak HXRBS)	58	10856	7579	4.0	19	1.75±0.02	1.73±0.02	0.96	1.46	0.56	1.03
Peak HXRBS	41	6223	3979	3.8	31	1.69±0.03	1.70±0.02	1.18	1.86	1.12	1.09
Peak BATSE	0	7234	4996	3.3	501	1.91±0.03	1.81±0.02	3.18	4.39	0.78	1.11
Peak RHESSI	0	7996	4399	3.7	20	1.87±0.03	1.86±0.02	1.28	2.00	0.77	1.88
Peak RHESSI (A16)	0	290	149	1.7	822	2.44±0.19	2.28±0.13	0.70	1.07	0.81	1.45
Counts HXRBS	2	8129	3314	4.6	3100	1.72±0.03	1.66±0.02	1.54	2.68	0.65	1.40
Counts BATSE	0	2748	2748	4.8	2000	1.48±0.03	1.50±0.03	1.67	5.20	2.94	1.07
Counts RHESSI	0	11548	8081	4.9	4783	1.60±0.02	1.64±0.02	3.34	10.98	2.77	1.54
Counts RHESSI (A16)	0	289	147	1.8	1.42×10^6	2.40±0.19	2.00±0.12	1.17	1.95	1.95	1.63
Duration HXRBS	2	11539	4341	2.2	126	2.61±0.04	2.66±0.02	4.43	5.45	1.58	0.90
Duration BATSE	0	7241	4562	2.1	37	2.32±0.03	2.19±0.03	5.65	5.81	0.00	1.77
Duration RHESSI	0	11445	8296	2.2	25	2.05±0.02	1.90±0.02	7.59	8.28	10.19	0.93
Duration (A14)	0	171	123	1.3	0	2.76±0.24	2.73±0.21	0.58	0.83	0.56	1.15
Duration (A16)	0	289	189	1.0	0	3.22±0.22	3.33±0.20	1.53	1.49	0.64	1.83
Length (A14)	0	171	112	0.9	26	5.13±0.44	5.03±0.38	1.10	0.52	0.55	1.25
Length (A15)	0	389	210	0.8	8	4.23±0.27	4.45±0.23	1.18	1.00	1.04	0.95
Area (A14)	0	171	100	1.5	899	2.84±0.27	2.82±0.22	0.71	1.05	0.73	1.75
Volume (A14)	0	171	96	2.2	30300	2.32±0.22	2.09±0.16	0.94	1.34	0.68	3.08
Volume (A15)	0	389	239	2.1	640	1.83±0.12	1.86±0.09	0.56	0.72	0.55	1.07
Magnetic energy (A14)	0	171	68	1.1	119	3.04±0.34	2.83±0.22	1.11	0.92	0.65	0.92
Nonthermal energy (A16)	0	192	89	2.6	0.32	2.50±0.25	1.59±0.11	1.28	2.34	2.08	1.87
Thermal energy (A15)	0	390	279	1.8	3	2.15±0.13	2.16±0.11	0.86	0.73	0.73	1.02
Emission measure (A15)	0	391	251	1.4	6.5×10^8	2.97±0.19	2.82±0.14	0.86	0.58	0.49	1.00
<u>Stellar flares:</u>											
Peak KEPLER	0	208	124	2.8	60255	1.66±0.14	1.68±0.12	0.81	1.26	1.45	3.55
Bolom. KEPLER	0	1537	727	1.5	3.8×10^{34}	2.56±0.09	2.55±0.07	1.31	2.18	0.67	0.97
<u>Terrestrial data:</u>											
Earthquakes	1	17425	9423	4.6	100	1.80±0.02	1.85±0.01	2.22	3.11	1.45	2.82
Fires	1	55853	38190	5.3	2	1.56±0.01	1.53±0.01	13.90	30.65	30.93	0.92
Cities	0	19445	12784	4.0	501	1.79±0.02	1.79±0.01	5.69	18.37	14.18	1.79
Blackouts	0	209	134	1.7	50000	1.98±0.16	1.90±0.13	0.80	0.83	0.63	3.35
Terrorism	1	2699	1949	2.4	2	2.48±0.05	2.28±0.04	4.86	2.25	0.43	6.15
Words	1	6609	4980	3.6	1	2.15±0.03	1.99±0.02	6.31	3.33	1.09	1.99
Surnames	2	2280	1663	2.2	15700	2.55±0.06	2.50±0.05	1.10	1.89	1.34	1.13
Weblinks	1	9.4×10^7	5.9×10^7	2.4	4	2.47±0.03	2.39±0.01	4.39	223	0.67	1.07

Table 2: Theroetically predicted power law slopes of solar flare size distributions (second and third column), which depend on the Euclidean dimension (S), the fractal dimension (D_S), the diffusion power exponent (β), and the energy-volume scaling exponent (γ), predicted by the fractal-diffusive SOC model (Aschwanden 2013). The power law slopes fitted to observed data sets (HXRBS, BATSE, RHESSI) are listed in the fourth column. Measurements with poor statistics and less reliable values are marked with parenthesis (...), obtained from the data sets A14, A15, and A16 (Aschwanden et al. 2014, 1015, 2016).

Parameter	Power law exponent (general expression)	Porwer law exponent $S = 3, \beta = 1, \gamma = 1,$ $D_2 = 3/2, D_3 = 2$	Power law exponent of observed solar flares α_x	Data set
Length L	$\alpha_L = S$	$\alpha_L = 3.00$	$\alpha_L = (4.45 \pm 0.23)$	A15
Length L	$\alpha_L = S$	$\alpha_L = 3.00$	$\alpha_L = (5.03 \pm 0.39)$	A14
Area A	$\alpha_A = 1 + (S - 1)/D_2$	$\alpha_A = 2.33$	$\alpha_A = (2.82 \pm 0.22)$	A14
Magnetic energy E_{mag}	$\alpha_{mag} \approx \alpha_A$	$\alpha_A = 2.33$	$\alpha_{mag} = (2.83 \pm 0.22)$	A14,A16
Emission measure EM	$\alpha_{EM} \approx \alpha_A$	$\alpha_A = 2.33$	$\alpha_{EM} = (2.82 \pm 0.14)$	A15
Bolom. energy E_{bol}	$\alpha_{bol} \approx \alpha_A$	$\alpha_A = 2.33$	$\alpha_{bol} = 2.55 \pm 0.07$	KEPLER
Volume V	$\alpha_V = 1 + (S - 1)/D_3$	$\alpha_V = 2.00$	$\alpha_V = (2.09 \pm 0.16)$	A14
Volume V	$\alpha_V = 1 + (S - 1)/D_3$	$\alpha_V = 2.00$	$\alpha_V = (1.86 \pm 0.09)$	A15
Thermal energy E_{th}	$\alpha_{E_{th}} \approx \alpha_V$	$\alpha_V = 2.00$	$\alpha_{th} = (2.16 \pm 0.11)$	A15,A16
Time duration T	$\alpha_T = 1 + (S - 1)\beta/2$	$\alpha_T = 2.00$	$\alpha_T = 2.66 \pm 0.03$	HXRBS
Time duration T	$\alpha_T = 1 + (S - 1)\beta/2$	$\alpha_T = 2.00$	$\alpha_T = 2.19 \pm 0.03$	BATSE
Time duration T	$\alpha_T = 1 + (S - 1)\beta/2$	$\alpha_T = 2.00$	$\alpha_T = 1.90 \pm 0.02$	RHESSI
Time duration T	$\alpha_T = 1 + (S - 1)\beta/2$	$\alpha_T = 2.00$	$\alpha_T = (2.73 \pm 0.21)$	A14,A16
Peak flux P	$\alpha_P = 1 + (S - 1)/(\gamma S)$	$\alpha_P = 1.67$	$\alpha_P = 1.70 \pm 0.02$	HXRBS
Peak flux P	$\alpha_P = 1 + (S - 1)/(\gamma S)$	$\alpha_P = 1.67$	$\alpha_P = 1.81 \pm 0.02$	BATSE
Peak flux P	$\alpha_P = 1 + (S - 1)/(\gamma S)$	$\alpha_P = 1.67$	$\alpha_P = 1.86 \pm 0.02$	RHESSI
Peak flux P	$\alpha_P = 1 + (S - 1)/(\gamma S)$	$\alpha_P = 1.67$	$\alpha_P = (2.28 \pm 0.13)$	A16
Peak flux P	$\alpha_P = 1 + (S - 1)/(\gamma S)$	$\alpha_P = 1.67$	$\alpha_P = (1.68 \pm 0.12)$	KEPLER
Fluence C	$\alpha_C = 1 + (S - 1)/(\gamma D_S + 2/\beta)$	$\alpha_C = 1.50$	$\alpha_C = 1.67 \pm 0.02$	HXRBS
Fluence C	$\alpha_C = 1 + (S - 1)/(\gamma D_S + 2/\beta)$	$\alpha_C = 1.50$	$\alpha_C = 1.50 \pm 0.03$	BATSE
Fluence C	$\alpha_C = 1 + (S - 1)/(\gamma D_S + 2/\beta)$	$\alpha_C = 1.50$	$\alpha_C = 1.64 \pm 0.02$	RHESSI
Fluence C	$\alpha_C = 1 + (S - 1)/(\gamma D_S + 2/\beta)$	$\alpha_C = 1.50$	$\alpha_C = (2.00 \pm 0.12)$	A16
Nonthermal energy E_{nth}	$\alpha_{E_{nth}} \approx \alpha_C$	$\alpha_C = 1.50$	$\alpha_{E_{nth}} = (1.59 \pm 0.12)$	A16

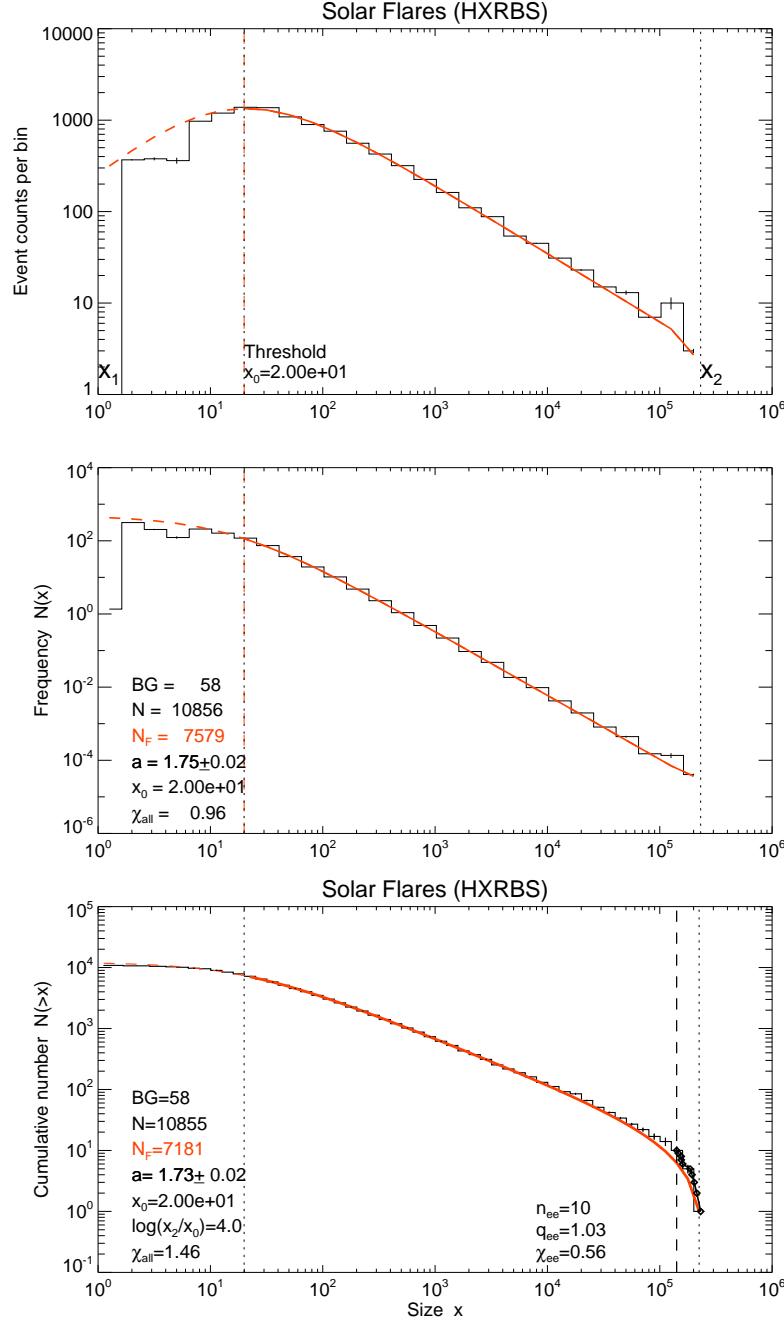


Fig. 1.— The statistics of solar flare hard X-ray peak photon rates are given in form of a histogram with the number of events per logarithmic bin (a), the differential occurrence frequency distribution (b), and the cumulative occurrence frequency distribution (c), with the rank-order plot overlayed for the 10 most extreme events (black diamonds). The observed data are shown in form of black histograms, while the fitted thresholded power law function is shown with a red curve. The data range $[x_1, x_2]$ is marked with dotted vertical lines, and the threshold value $[x_0]$ with a dotted dashed line. The least-square fit criterion is calculated for the entire distribution sampled above the threshold ($\chi_{all} = 1.46$), and for the range of extreme events ($\chi_{ee} = 0.56$).

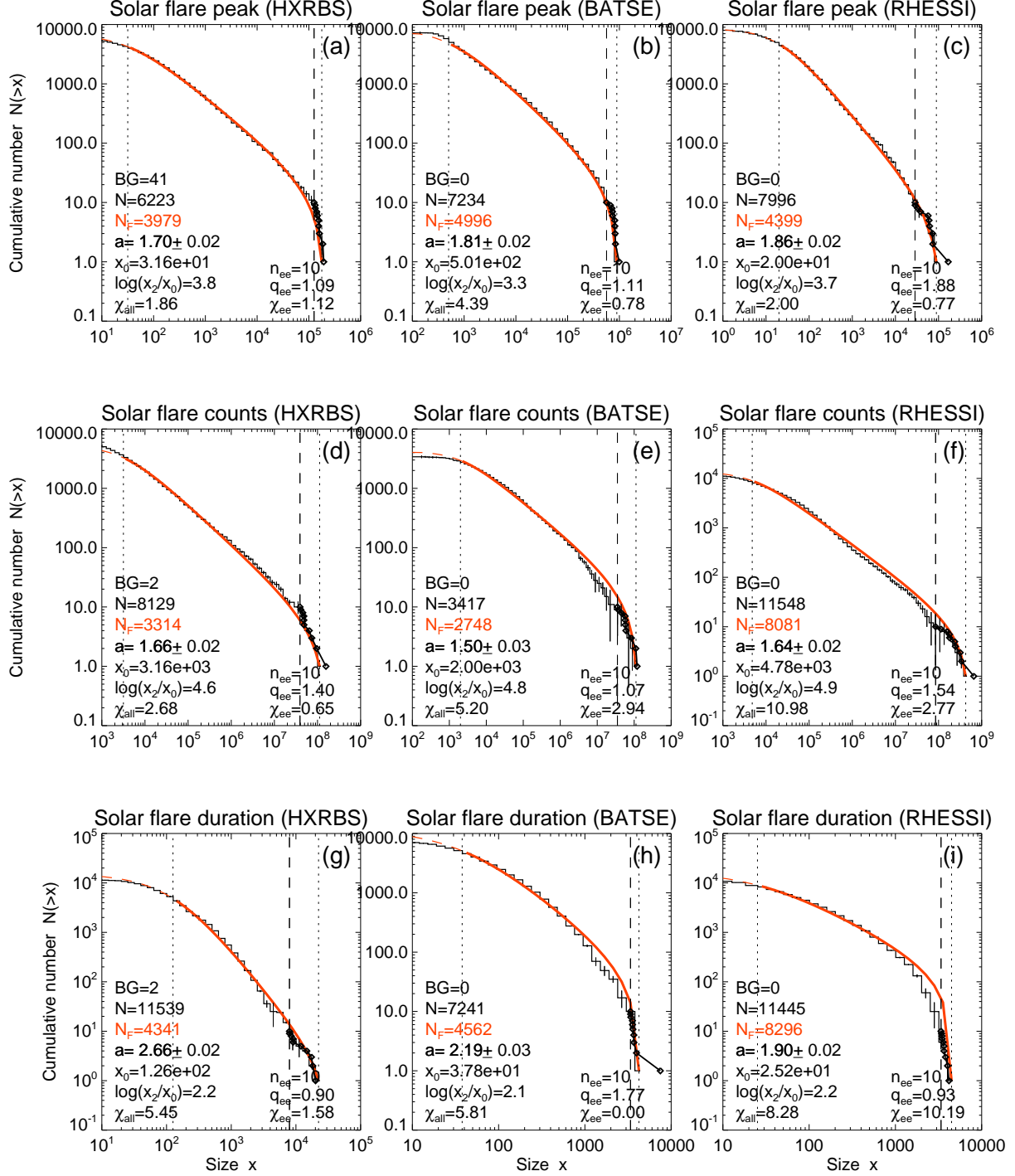


Fig. 2.— Solar flare hard X-ray peak photon rates (a-c), fluences or counts (d-f), and flare durations (g-i) are histogrammed from HXRBS observations (a, d, g), BATSE observations (b, e, h), and RHESSI observations (c, f, i) (shown in form black histograms with uncertainties), and in form of the best-fit cumulative distribution functions (red curves). The chi-square is given for all events above the threshold x_0 , $\chi_{all}(x > x_0)$, and for the 10 most extreme events separately, $\chi_{ee}(x > x_3)$.

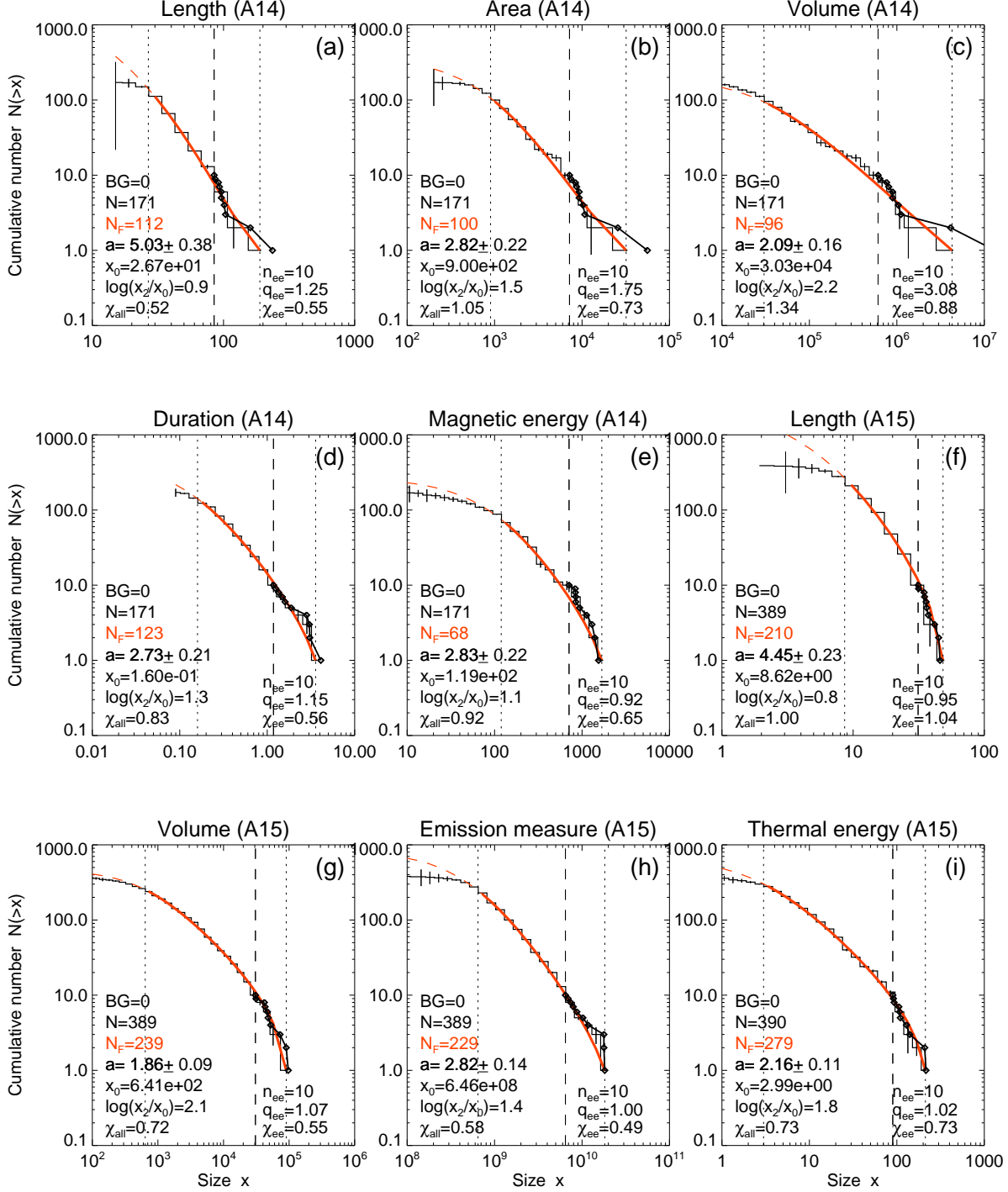


Fig. 3.— The cumulative size distributions of solar flare quantities are shown for length scales (a, f), flare areas (b), flare volumes (c, g), flare durations (d), the dissipated magnetic energy (e), the EUV emission measure (h), and the thermal energy (i), calculated in two previous works (Aschwanden et al. 2014, 2015). Representation otherwise similar to Fig. 2).

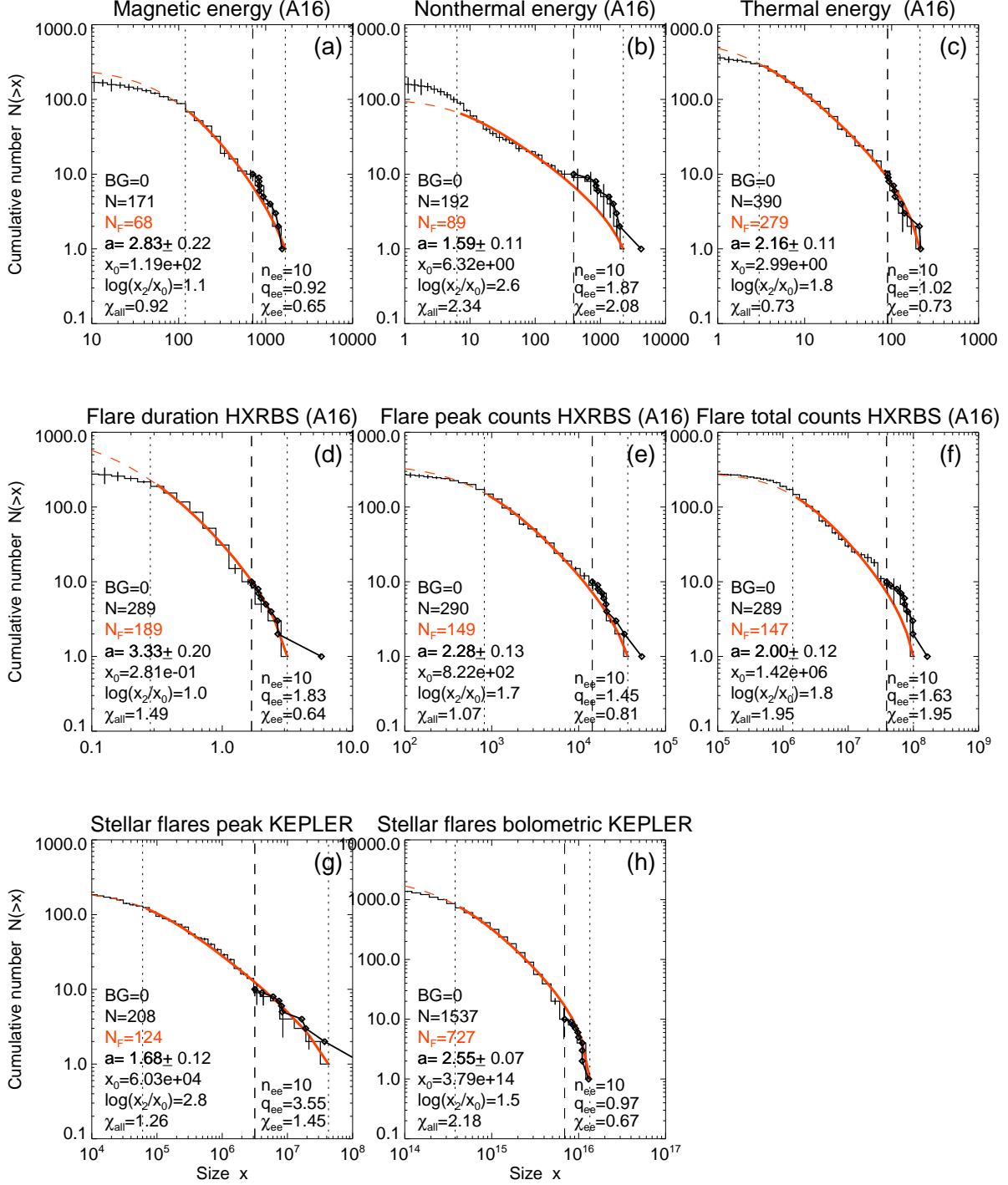


Fig. 4.— The cumulative size distributions of solar flare quantities are shown for the dissipated magnetic energy (a), the nonthermal energy (b), the thermal energy (c), flare durations (d), peak counts (e), total counts (f), the peak intensity of stellar flares (g), and the stellar bolometric energy of stellar flares (h), calculated from two previous works (Aschwanden et al. 2016). Representation otherwise similar to Fig. 2).

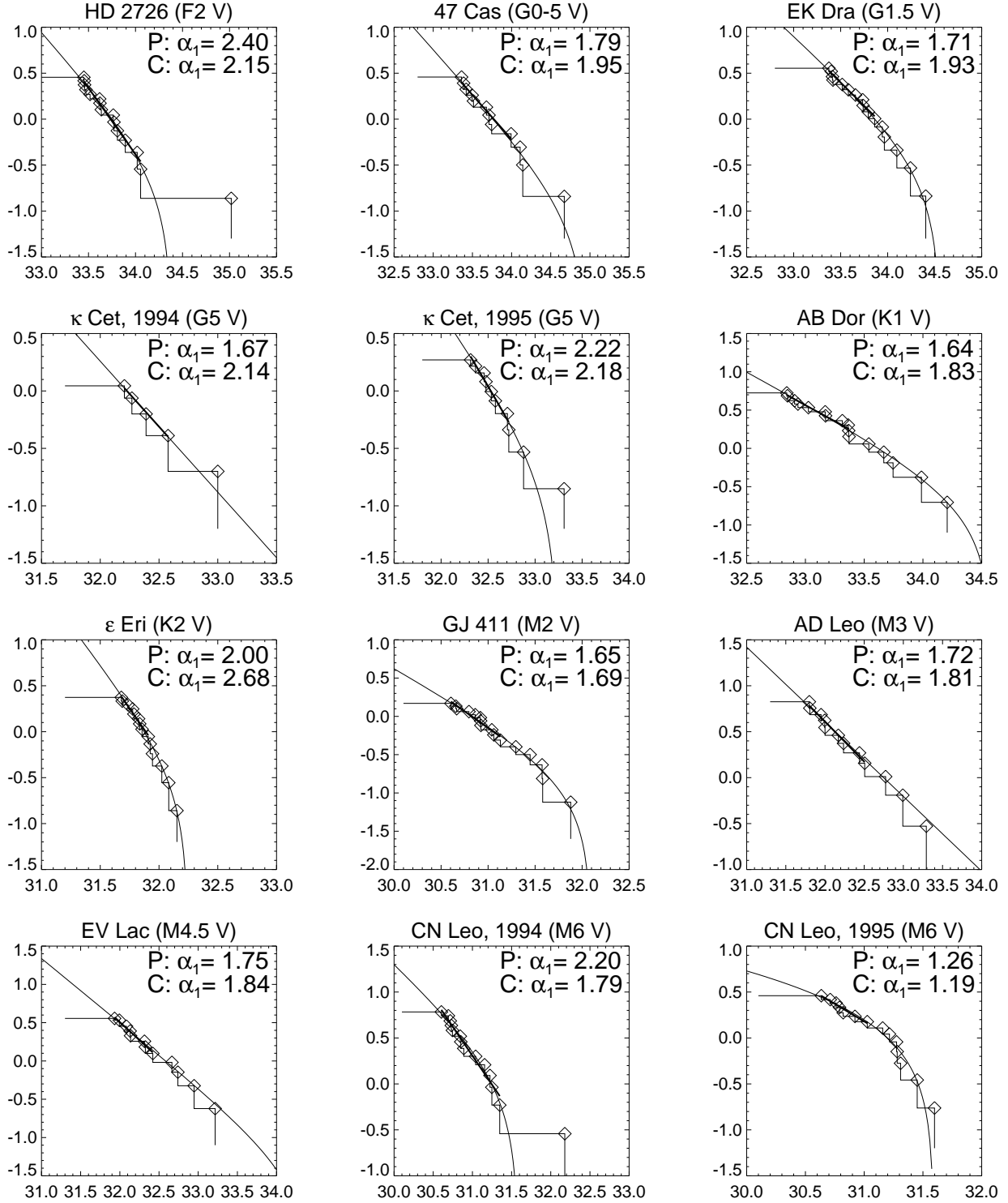


Fig. 5.— Cumulative frequency distributions of flare energies (total counts) observed for 12 cool (type F to M) stars with EUVE (Audard et al. 2000). The flare events are marked with diamonds, fitted with a power law fit in the lower half (P; thick line), and fitted with a cumulative frequency distribution (C; curved function). Note two stars with outliers at the largest events (HD 2726) and (CN Leo, 1994).

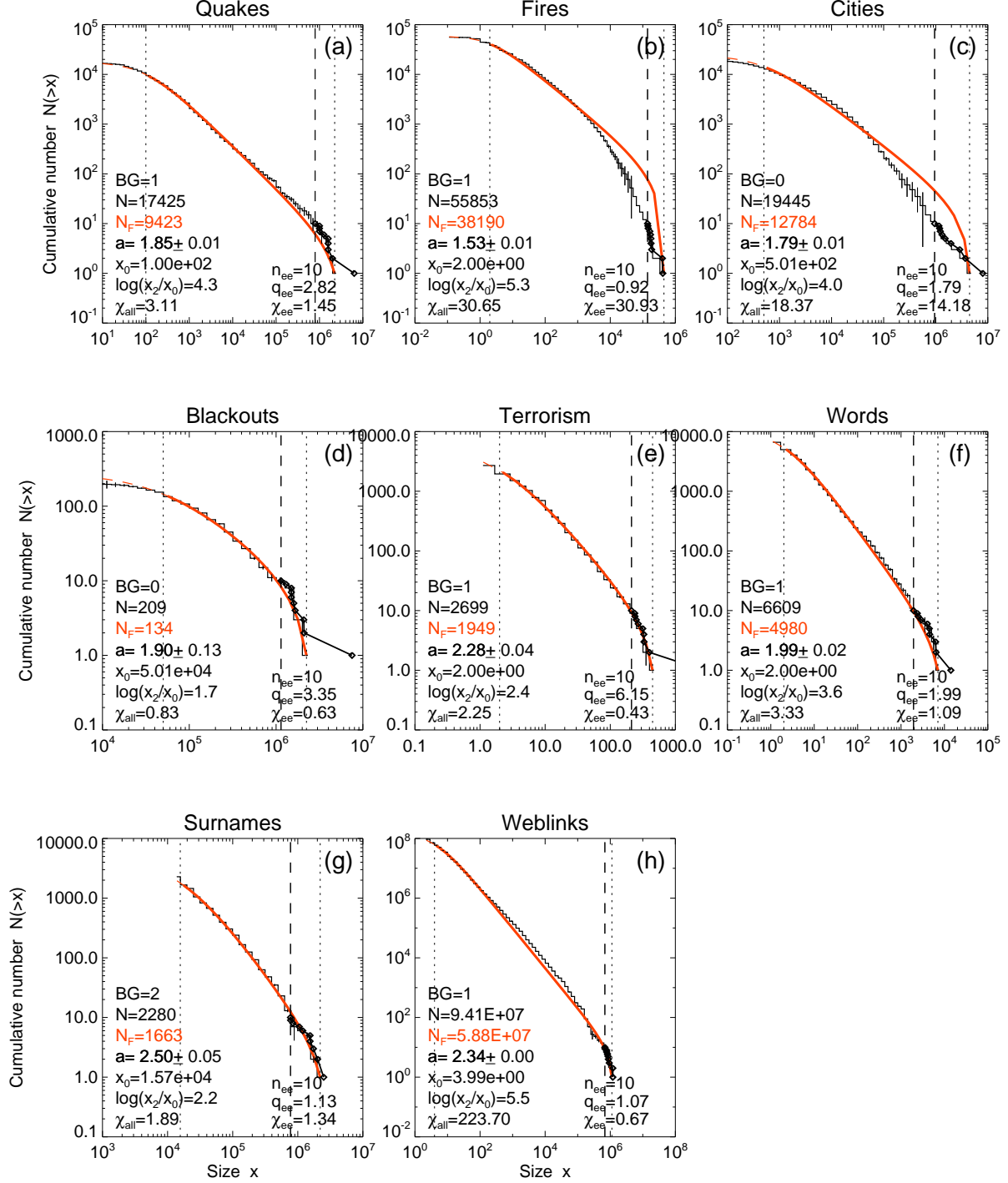


Fig. 6.— Cumulative size distributions are shown for 8 empirical data sets from Clauset et al. (2009): Earthquake intensities (a), forest fires (b), population of cities (c), electric power blackouts (d), terrorist attack severity (e), count of words (f), frequency of surnames (g), and links to web sites (h). Representation otherwise similar to Figs. 2-4.